POAC'13
Espoo, Finland

Proceedings of the 22nd International Conference on
Port and Ocean Engineering under Arctic Conditions
June 9-13, 2013
Espoo, Finland

FACTORS INFLUENCING MANAGED SEA ICE LOADS

Martin Richard [1,2] and Richard McKenna [1,3]
[1] Centre for Arctic Resource Development (CARD), St. John's, NL Canada
[2] C-CORE, St. John's, NL Canada
[3] R.F. McKenna Associates, Wakefield, QC Canada

ABSTRACT
Sea ice management has an important role in enabling the movement of vessels through heavy ice conditions and in reducing the severity of ice interactions with floating systems. Except for analyses of managed ice conditions and loads from the Kulluk drilling vessel, the factors influencing loads from managed ice have received relatively little attention. Ice thickness, the presence of pressure ridges and the average floe size of managed ice are important factors while other features of the ice cover such as floe size distribution and station-keeping system characteristics are also important. This paper focuses on the dynamics of a broken ice field and the displacements of a station-keeping vessel in the horizontal plane using a new two-dimensional discrete element model. The discrete element approach simulates the complex dynamics of the broken ice field and is used here to assess the sensitivity of different scenarios on loads experienced by the station-keeping system. The model approximates the shape of managed sea ice floes by circular discs of random diameters. The mechanics of the broken ice field is driven by the contact forces between individual floes. A viscoelastic contact model is used with boundary conditions and environmental forcings that vary both in time and space. The influence on loads of (1) floe size distribution; (2) stiffness of the station-keeping system; and (3) changes in ice drift direction are examined. The ability to correctly model these factors is critical for effective ice management operations. The results of the study highlight the relative importance of those factors for evaluating operational ice management strategies and for defining operating envelopes.

INTRODUCTION
Effective ice management is necessary for floating systems operating in heavy sea ice conditions. Typically, icebreakers are used to break up large floes or thick ice features approaching the facility in order to reduce the pressure and concentration of ice surrounding the facility. The extent of ice management required to stay safely on location is determined by the ice conditions, the environmental conditions, the ice management capabilities and the station-keeping system.

The ability to accurately model ice loads on a floating system subjected to ice management operations is of considerable importance. The magnitudes of the loads as well as the ice dynamics around the vessel under different conditions (i.e., ice, atmospheric and oceanographic conditions) are important considerations. Research and development in this area seeks to extend the ice conditions in which station-keeping is possible, extend the seasonal operational window and reduce the ice management effort.

Except for analyses of data from the Kulluk drilling vessel (Wright, 1999), the factors influencing loads from managed ice have received relatively little attention. Ice thickness, the presence of pressure ridges and the average floe size of the managed ice are important factors but other features of the ice cover such as floe size distribution and station-keeping system characteristics are also important. This paper focuses on the dynamics of a broken ice field and the displacements of a moored vessel in the horizontal plane using a two-dimensional discrete element model.

A discrete element model has been developed to investigate the effect of (1) floe size distribution; (2) stiffness of the station-keeping system; and (3) changes in ice drift direction, on the ice loads and ice regime around a moored vessel. This is a first step in modelling operational situations to determine which ice features pose the greatest threat in combination with weather and oceanographic conditions, the severity of the threats and the probability of impact. This information could then be used to coordinate physical ice management and station-keeping operations (e.g., move or rotate the vessel in anticipation of given incoming ice conditions; disconnect if the management cannot keep up with changing conditions, etc.).

NUMERICAL MODELLING

Discrete Element Representation of the Ice Field

Since the Discrete Element Method (DEM) was developed by Cundall and Strack (1979) to model granular assemblies, it has been applied in many fields and for many different purposes. Applications to ice engineering include modelling river ice (Daly and Hopkins, 1999); broken ice field and discrete ice floes (Løset, 1994a, 1994b; Sayed et al., 1995); moored systems in broken ice (Hansen and Løset, 1999a, 1999b); sea ice at the mesoscale (Hopkins, 2004); ice ridging (Hopkins, 1994); ice rubble formation (Paavilainen et al., 2011); and ice ridge keel punch tests (Polojärvi and Tuhkuri, 2009).

In the present paper, a two-dimensional horizontal discrete element model is used to simulate the complex dynamics of a managed ice field upstream of a moored production facility. The current version of the model approximates the shape of sea ice floes by circular discs (*particles*), with a specified size distribution. The mechanics of the broken ice field is driven by the contact forces between individual floes and the boundaries. The forces for two particles that are in contact or particles in contact with a boundary are calculated using a soft contact model, i.e., the intersecting area (or overlap) between two (or more) particles (or boundary) is interpreted as a small deformation of rigid bodies. In the present version of the model, a repulsive force between the particles (or the boundary) is generated using a standard viscoelastic contact model, as used in Babić (1988). The force in the normal direction consists of an elastic term (spring) and a viscous damping (dashpot) term. The force in the tangential direction is modelled as viscoelastic below the friction limit and frictional at the friction limit. The friction is assumed to follow a Mohr-Coulomb law. The normal (F_n) and tangential (F_s) forces are given by:

$$F_n = K_n \delta_n + C_n \dot{\delta}_n \tag{1}$$

$$\begin{cases} F_s = K_s \delta_s + C_s \dot{\delta}_s & \text{for } |K_s \delta_s| \le |\mu F_n| \\ F_s = sign(K_s \delta_s)|\mu F_n| & \text{for } |K_s \delta_s| > |\mu F_n| \end{cases} \tag{2}$$

where K_n and K_s are respectively the effective normal and shear contact stiffnesses ($K_{n,s}^{ij} = k_{n,s}^i k_{n,s}^j / \left(k_{n,s}^i + k_{n,s}^j\right)$, where i and j refer to the two particles in contact and k is either in the normal or tangential direction); δ_n and δ_s are the overlap in the normal and tangential directions; $\dot{\delta}_n$ and $\dot{\delta}_s$ are the displacement rates; C_n and C_s are the normal and shear damping coefficients (proportional to $\sqrt{mK_{n,s}}$); and μ is a coefficient of friction. The magnitude of the shear force is not allowed to exceed $|\mu F_n|$. If it does exceed that limit, the viscous damping in the shear direction is not applied.

For the simulations presented in this paper, $k_n = 1$ x 10^6 N/m and $k_s = 0.38$ x 10^6 N/m (i.e., $k_s = k_n\left(2(1+\nu)\right)^{-1}$, where ν is Poisson's ratio (Hansen and Løset, 1999a). For particles colliding with the vessel, a smaller value for k_n was used (1 x 10^5 N/m). The k_n-value is important in that it determines the ice loads on the vessel. From some test runs results, it was

noticed that increasing the k_n-value by an order of magnitude could increase the global ice loads on the vessel by a factor of 2-3. The dominant mechanism for ice failure against the vessel is likely to be flexural failure (due to the sloped bow), as opposed to crushing, splitting rubbling or rafting failures which would be expected to occur in the plane of the ice (and result in larger interaction forces), hence the smaller k_n-value for the ice-vessel contacts compared to ice-ice contacts. It is believed that these k_n-values are of the right order of magnitude in order to produce realistic force levels; to approximate the behaviour of the ice; and to illustrate the sensitivity to parameters studied in this paper. The intent here is not to promote these pressures and loads for design. Refinements of the model are planned in order to add more realism to the model.

For a particle-particle contact, the normal force does not produce a moment (because of the circular shape). In cases where a contact between a particle and a linear boundary segment is partial (i.e., the linear segment does not go entirely through the particle), a moment is generated from the normal force as well as the tangential force, based on an assumed pressure distribution over the width of the contact area.

Drag forces exerted by the wind and current on ice pieces were calculated with standard quadratic drag laws with constant drag coefficients of 0.015 for wind drag and 0.010 for current drag. Based on the calculated forces acting on each particle and on the vessel, the accelerations are calculated by solving Newton's equations, after summing the applied forces (ice, boundary, mooring lines, current and wind), using an explicit central difference time integration scheme (Munjiza, 2004).

Vessel and Mooring System

The forces acting on the vessel are calculated in the vessel's local frame of reference following x' and y', for which x' is the bow direction and y' is the port direction. The wind and current angles are positive counterclockwise from the x'-axis and are both given as 'direction towards'. The modelled vessel used for the simulations has a waterline length of 260 m, a waterline beam at mid-ship of 46 m, draft at mid-ship of 12 m, a deadweight tonnage of 139,000 tons, a mass moment of inertia about the yaw axis of 5 x 10^{12} kg^1m^2 and a block coefficient of 0.85. The turret is located 175 m fore of stern.

The wind and current forces and yaw moments acting on the vessel are calculated with (based on Journée and Massie, 2001):

$$F_D = 0.5\rho U_{rel}^2 A_{eff} C_D \qquad (3)$$

in which F_D can stand for either $F_{x'}^{wind}$, $F_{y'}^{wind}$, M^{wind}, $F_{x'}^{current}$, $F_{y'}^{current}$ and $M^{current}$, which are the wind and current longitudinal (following x') and lateral (following y') forces and yaw moments. The density used (ρ) is that of the air or the water, for calculation for wind and current respectively. Similarly, the relative velocity (U_{rel}) is that between the vessel and the air or the current. A_{eff} is the effective area for drag forces calculations or effective area multiplied by the moment arm, for moments calculations. For calculation of $F_{x'}^{wind}$ and $F_{y'}^{wind}$, A_{eff} is the transverse (A_T) or lateral (A_L) projected wind area, respectively. For calculation of M^{wind}, $A_{eff} = A_L L$, where L is the vessel length. The force coefficients and the yaw moment coefficients all depend on the relative angle between the vessel's local x'-axis and the direction of the wind or current (Figure 1). For calculation of $F_{x'}^{current}$, $A_{eff}C_D = A_P C_{x'}^{prop} + TBC_{x'}^{form} + SC_{x'}^{friction}$, where A_P is the propeller expanded blade area; T and B are respectively the vessel's draft and beam; and S is the vessel's wetted surface (USACE, 2005). Calculations of $F_{y'}^{current}$ and $M^{current}$ are made with $A_{eff} = A_{LS}$ and $A_{eff} = A_{LS}L$, where A_{LS} is the submerged lateral projected area.

The mooring system is assumed to be made of an array of catenary lines that are attached to the vessel at the location of the turret. For simplicity, the same three assumptions as in Hansen and Løset (1999a) are made: (1) the drag on the lines is neglected; (2) the tension in the line only depends on the relative position of the vessel; and (3) the line response is quasi-static.

For operations in shallow water, such as the case of the Kulluk drilling barge (Wright, 1999), the mooring system is usually very stiff in order to avoid the facilities moving too far off location (typically, the acceptable range for a drilling vessel is close to 5% of the water depth, which, for a depth 75-100m would give a tolerable offset value of about 4-5m). In the present version of the model, the restoring force as a function of the excursion is assumed linear. The system is simplified with an equivalent spring (representing a set of mooring lines) in both the x and y directions and the stiffness values for both directions are the same (it is assumed that the mooring system has a symmetric behaviour). The restoring forces are applied at the turret location and therefore induce a rotational moment on the vessel.

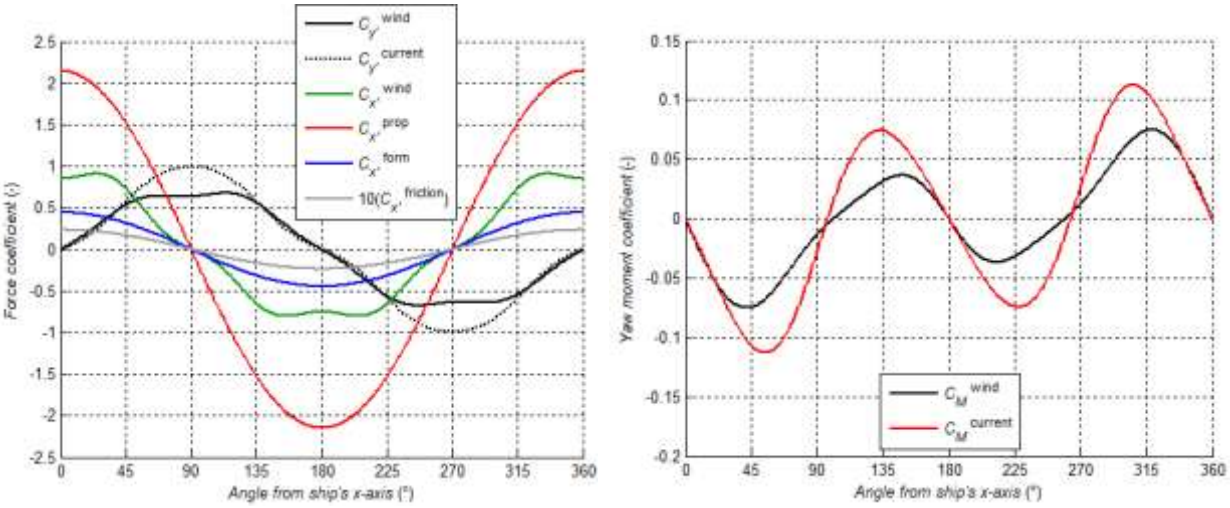

(a) (b)

Figure 1. (a) Force coefficients and (b) yaw moment coefficients as a function of the wind or current relative angle with the vessel

TEST CASES AND DISCUSSION

Influence of floe size and distribution

Wright (1999, 2000) has reported managed floe sizes at the Kulluk platform that range between 30 and 100 m and, for ice that was well managed, between 10 and 60 m, with thicknesses in the range of 1.2 to 3 m. For the current simulations, a 'managed ice channel' 1000 m wide was populated with an ice concentration of about 75% by floes defined by a lognormal distribution having a mean of 45 m and a standard deviation of 20 m. A lower cutoff in the distribution was set to 10 m in order to avoid the spurious dynamics that were found when including such small ice pieces. This truncation (along with the idealized circular shapes of the floes) means that the reported concentration is to be seen as 'modelled concentration'.

An upper limit in floe diameter was also applied. The floe diameter distribution was truncated at the upper level. The upper cutoff was varied as an analogue for the efficiency of the ice management operations, i.e., how efficient the icebreakers are in breaking the floe population into smaller pieces; if some floes are too large or thick to be managed or insufficient time is available to further break up the floes, for example. For the simulations, the upper cutoff was varied between 60 m and 120 m.

All floe thicknesses were assumed to be 1 m. The turret on the vessel was initially positioned at the origin (in the global frame of reference) and the vessel's local x'-axis was defined by the unit vector [1 0], i.e., the vessel's heading is 90° from the horizontal (positive counterclockwise). Two rigid boundaries were imposed on the side of the simulation area (at $x = \pm 500$) so that the managed ice is restrained to flow into the virtual 'managed ice channel' (this influences the surrounding ice pressure for the current scenarios). Steady and spatially uniform wind and currents were used. The u-v components of the current were set to 0 and -1 m/s respectively and those for the wind were set to 0 and -5 m/s. The distances between the turret and the station (i.e., initial position of the turret) are used as the excursion values to calculate the restoring force induced by the mooring lines. The mooring stiffness ($K_{mooring}$) was set constant to 0.4 MN/m for the four runs considered in this section.

Figure 2 shows an example of a short time series of the ship's ice resistance. The ice resistance refers to the sum of all longitudinal (i.e., following the x'-axis) ice forces applied on the ship. The ice loads applied on both sides of the vessel are also shown (i.e., parallel to the direction of the y'- axis). In general, the model behaviour was satisfying although occasional 'bouncing' of the floes when they contact the vessel can sometimes be seen, as evidenced by the occasional load peaks seen in Figure 2. These features of the loading, which depend on the size and shape of the ice floes, the ice conditions around the vessel and on the contact model are still under investigation.

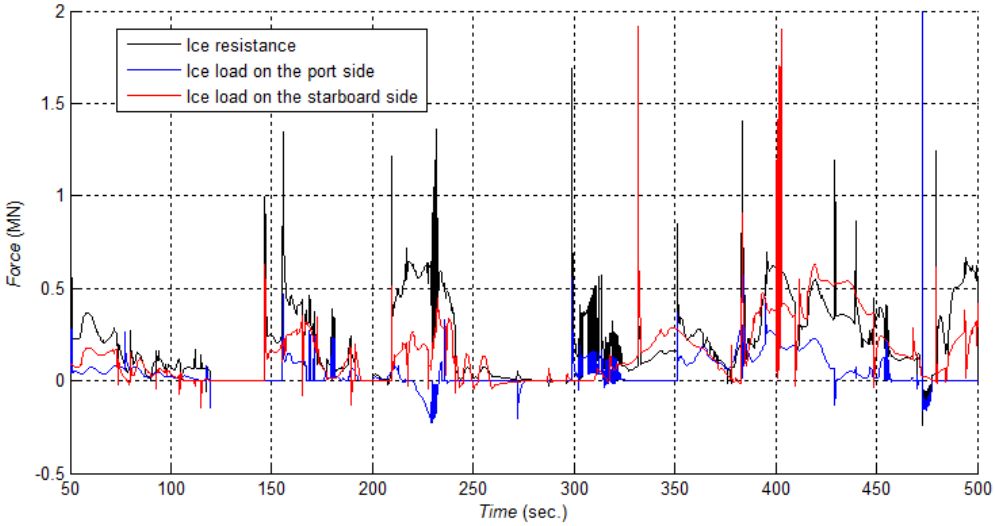

Figure 2. Example of a time series of ice resistance and ice loads applied on both sides for case with an upper cutoff of 60 m

Figure 3 shows the 95th percentile values of the global ice load applied on the vessel, the restoring force and the ice resistance, as a function of the floe diameter distribution upper cutoff to ship beam ratio (d^u/B). The global ice load is the magnitude of the resulting ice force acting on the vessel (i.e., sum of all forces from ice pieces). The restoring force is calculated by multiplying the magnitude of the excursion by the mooring stiffness. The ice resistance is as defined previously. On Figure 3, an additional scenario (the 'unmanaged ice' case) has also been added in order to show the effect of a much larger floe diameter distribution on the calculated loads.

For values of d^u/B below 3, there is an increase of global ice loads and ice resistance with increasing ratio. The restoring force data do not show a similar increase. However, for the case in unmanaged ice, loads are significantly higher for all force components. The mean global ice loads were roughly between 1/2 and 1/3 of the 95th percentile values and the standard deviations were slightly higher than the means. The excursion 95th percentile values

were in the order of 5-7 m and relatively constant for all cutoffs. For the 120 m cutoff, even though the 95th percentile value was similar to other cutoffs, the mean and standard deviation were significantly higher than for other cutoffs.

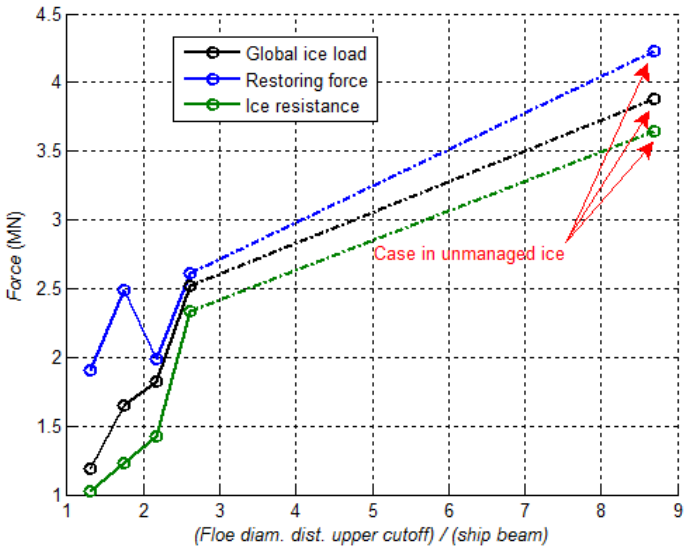

Figure 3. Force components (95th percentile) as a function of the floe diameter distribution upper cutoff to ship beam ratio (d^u/B)

Influence of the stiffness of the station-keeping system

Four runs with different equivalent stiffnesses for the mooring system ($K_{mooring}$ = 0.2, 0.4, 0.6 and 0.8 MN/m) were performed. Figure 4 shows the maximum (95th percentile) global ice loads, restoring forces, ice resistance and excursion values as a function of mooring stiffness, using the same distribution for the managed ice floe diameters as in the previous cases.

Excursion values decrease, as expected, with increasing mooring stiffness. The mean values varied between 1 m (for $K_{mooring}$ = 0.8 MN/m) and 3.4 m (for $K_{mooring}$ = 0.2 MN/m). The standard deviations were about half the mean values, except for the case with a stiffness of 0.2 MN/m, for which it was much higher (about 2.6 m). Those trends are also made apparent in Figure 5, which shows the position of the turret throughout the entire simulation for two different runs with different mooring stiffnesses as well as a time series of excursion for a portion of the simulations. Restoring force mean and standard deviation are approximately constant regardless of the mooring stiffness value. The 95th percentile values seem to decrease slightly with higher stiffness, but the data seem to show that restoring forces are independent of mooring stiffnesses. Large differences in excursion are seen for different mooring stiffnesses while the restoring forces are relatively constant. This is also shown as probability density functions (PDFs) in Figure 6.

Ice resistance and global ice loads were roughly constant for all stiffnesses. Based on the results of the simulations performed, the stiffness of the mooring system appears to have no effect, in a statistical sense, on the local (i.e., next to the vessel) ice dynamics (interaction between ice pieces and the way the ice float around the structure).

Figure 7a shows the power spectral density (represented by the ratio of the variance to the mean of the variance) of the excursion for the cases with mooring stiffness of 0.2 and 0.8 MN/m. The normalized variance peaks are found at frequencies of approximately 5.2x10^{-3} and 10x10^{-3} Hz, for stiffness values of 0.2 and 0.8 MN/m, respectively (which corresponds to periods of 191 and 100 sec.). The natural frequency of a spring-mass system is proportional to the square root of the stiffness ($f_n = (1/2\pi)(k/m)^{1/2}$), so that, the expected ratio for the two

stiffness analyzed here is 2 (i.e., $\sqrt{0.8}/\sqrt{0.2} = 2$). The frequencies in Figure 8a have a ratio of about 1.91 (i.e., $f^{K=0.8}/f^{K=0.2} = 0.01/0.0052 = 1.91$).On Figure 7b is also shown the power spectral density spectrum of the ice force on the vessel. The two main frequency peaks for the stiffness values of 0.2 and 0.8 MN/m, respectively, are $2x10^{-3}$ and $3.85x10^{-3}$ Hz (periods of 500 and 250 sec. respectively), for which the ratio is 1.93.

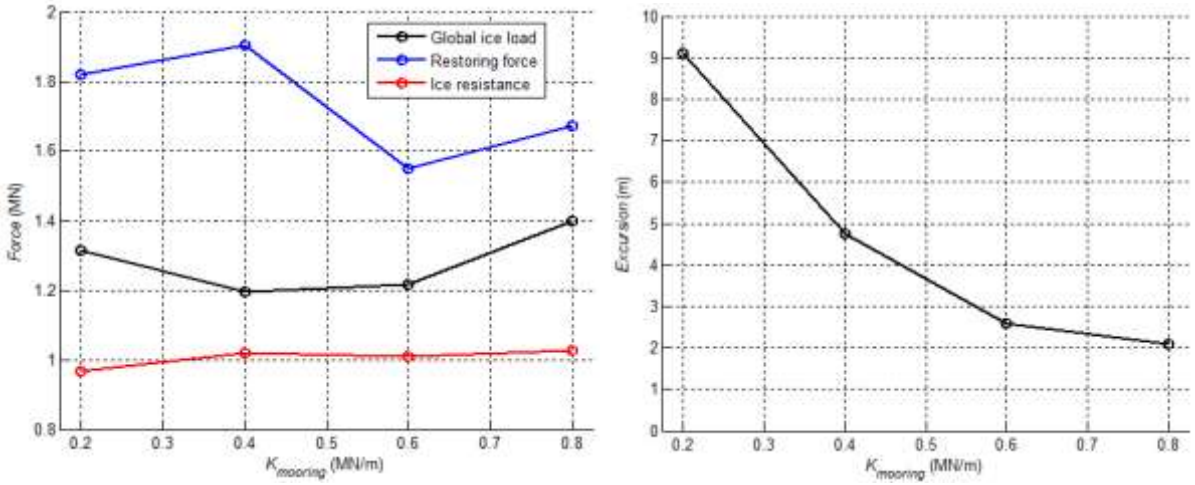

(a) (b)

Figure 4. (a) Force (95th percentile) exerted by the ice and mooring force as a function of mooring stiffness; and (b) total excursion (95th percentile) as a function of mooring stiffness

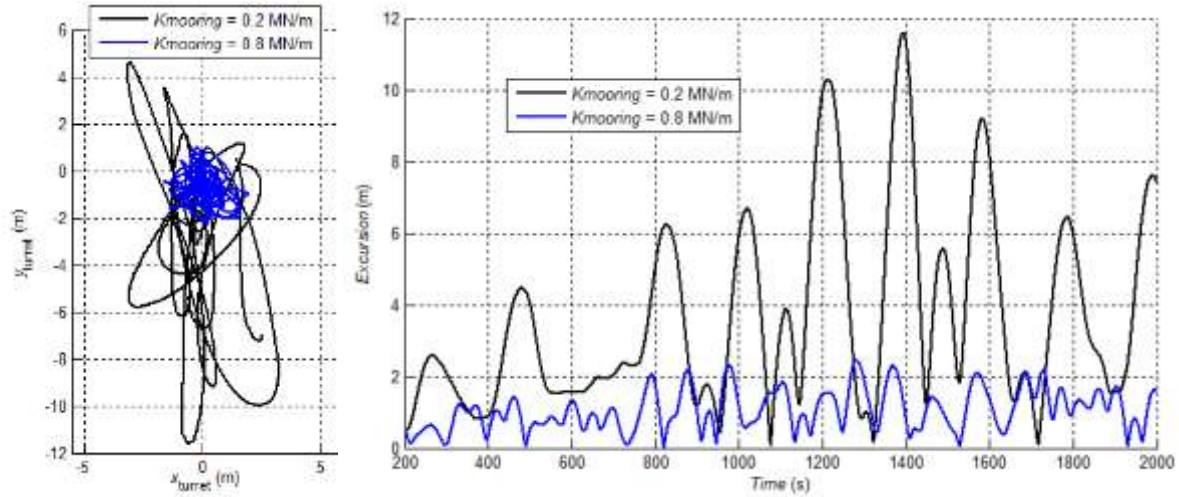

(a) (b)

Figure 5. (a) Turret position throughout the entire simulation; and (b) total excursion time trace for a portion of the simulations for two different mooring stiffness

The ratios of the main frequency peaks discussed were both close to the expected value of two, for both the excursion and the global ice load. However, the power spectrums show other peaks, which indicate the relative influence of other processes on the frequency content of those two parameters. In Figure 7b, the range of frequencies attributable to the ice contact model combined with sizes of ice pieces used is shown in the gray area (frequencies between $1.5x10^{-2}$ and $8.9x10^{-2}$ Hz). Also, it is worth noting that the two main frequency peaks of $5.2x10^{-3}$ and $10x10^{-3}$ Hz in the excursion power spectrum are also seen in that of the global ice loads. Other small peaks could be caused by a multitude of effects, such as rotational stiffness, lateral effects, etc.

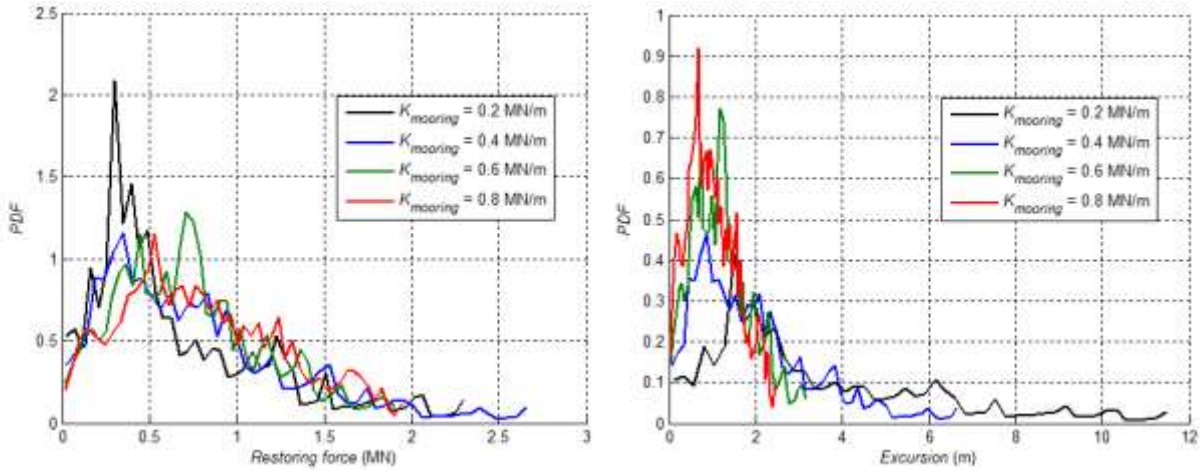

(a) (b)

Figure 6. Probability density function (PDF) of (a) mooring force and (b) excursion for four different mooring stiffness

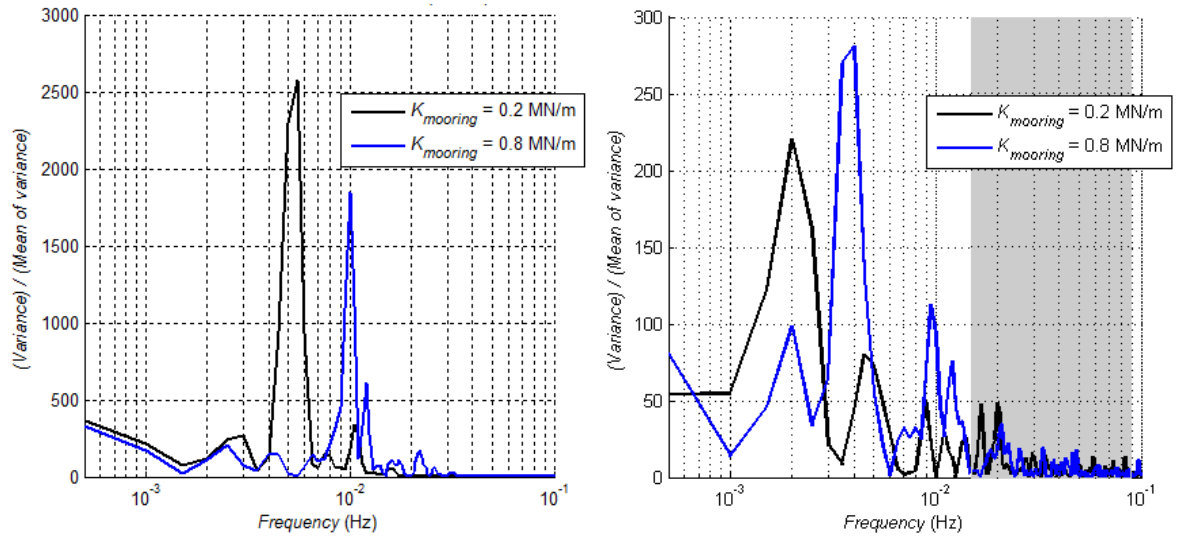

(a) (b)

Figure 7. Normalized (to the mean of the variance) power spectral density of (a) the excursion and (b) the global ice load

Influence of change in ice drift direction

Keinonen et al. (2006) note two kinds of deviation from station-keeping position: (1) sideways shift and (2) deviation of position in the direction of ice drift. When the ice drift direction changes, the vessel may experience different ice loads regimes. Moored vessels are often very difficult to manoeuvre quickly in order to react and in high concentrations of ice they can only weathervane slowly. In such circumstances, the capacity of the vessel to turn at a sufficient speed, the efficiency of the icebreakers to release pressure around the vessel and the length of the vessel are key components that will influence the ice loads the vessel will experience. Further, the width of the managed ice channel during drift direction changes can potentially influence the ice loads. In this section, the impact of setting the vessel closer to the unmanaged ice (i.e., offset from the centre of the managed ice channel); the capacity of the vessel to stay in the managed ice channel when a drift direction change occurs; and the changes in the ice load regime as the drift direction changes and as the vessel is set farther outside the managed ice channel are explored.

Three different sets of simulations were performed: (1) sideways shift of the vessel location relative to the centre of the managed ice channel, with a constant ice drift speed and direction; (2) vessel initially located at the centre of the managed ice channel, with a constant drift direction rate of change for a limited time; and (3) vessel initially located at the centre of the managed ice channel, with a complete loop in the ice drift direction. The managed ice channel was populated by floes having the same diameter distribution as in previous sections, with an upper cutoff of 60 m. A population of much larger floes (represented by a Weibull distribution with a mean of 125 m, a standard deviation of 50 m, a lower cutoff of 20 m and an upper cutoff of 400 m), serving as the unmanaged ice, was added on both sides of the managed ice channel. An example of the initial condition with the vessel centred in the channel (1 km wide) is shown in Figure 8.

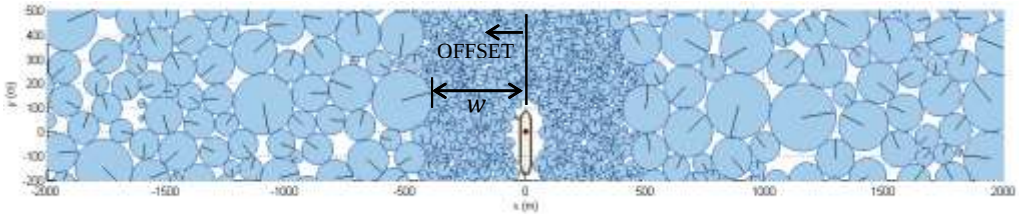

Figure 8. Example of initial condition

Sideways shift

Five different simulations were performed to evaluate the effect of the transverse position of the vessel in the managed ice channel. Given that the channel has a width of $2w$, the horizontal offset (following x) from the centre of the channel (an offset of 0 means it is centered while an offset of w means it is on the limit between managed and unmanaged ice, see Figure 8) was set to (1) 0 (i.e., centred); (2) $0.25w$; (3) $0.5w$; (4) $0.9w$; and (5) $2w$ (i.e., completely in the unmanaged ice). The environmental conditions were the same as in previous cases (i.e., wind and current directed parallel to y, in the negative direction). There were no additional boundaries around the unmanaged ice to restrain its movement.

Figure 9 shows, as a function of relative horizontal position of vessel with respect to the centre of the managed ice channel, the magnitude of the 95th percentile value of the global ice load applied on the vessel, restoring force, ice resistance and ice load on the port side of the vessel. A value of zero on the x-axis means that the vessel is centred whereas a value greater than one means that it is in the unmanaged ice. If the vessel is within the managed ice channel limits, there does not seem to be a significant influence of its relative position on the magnitude of the force components shown. The ice load applied on the port side (i.e., the side that is closer to the unmanaged ice in the simulations) seems to slightly increase as the distance to the unmanaged ice decreases, but not significantly enough to rule out that this is not caused by randomness. In unmanaged ice, all forces are significantly larger, except for the ice load applied on the port side (which shows less increase – the loads on the starboard side were similar).

Change in ice drift direction

To simulate changes in ice drift direction, the vessel was first positioned in the centre of the managed ice channel. The ice drift direction was rotated counterclockwise at three different rates between (36, 72 and 144 deg/hour). The 'virtual' trajectories (i.e., equivalent trajectories if the vessel would have been moving instead of the ice floes) of the vessel based on the applied ice drift direction rates is shown in Figure 10a.

Normally, for the smallest drift direction rates of change, the vessel was able to rotate about the turret in order to approximately follow the change in drift direction. For the 144 deg/hour

case, the forces resisting turning became too large when the current was almost 60° off its original direction for the vessel to continue its rotation. Also, for the same case, the vessel reached the unmanaged ice towards the end of the simulation, at which point the excursion values started to increase along with the ice loads.

Figure 10b presents the 95th percentile of the global ice loads, restoring force and ice resistance as a function of ice drift direction rate of change. These forces all increase with increasing drift direction rate of change. The slight drop in the slope of the ice resistance line as it goes towards the 144 deg/hour value is attributed to the fact that the vessel was unable to efficiently turn and follow the ice drift direction at one point in the simulation as the drift direction was changing too quickly.

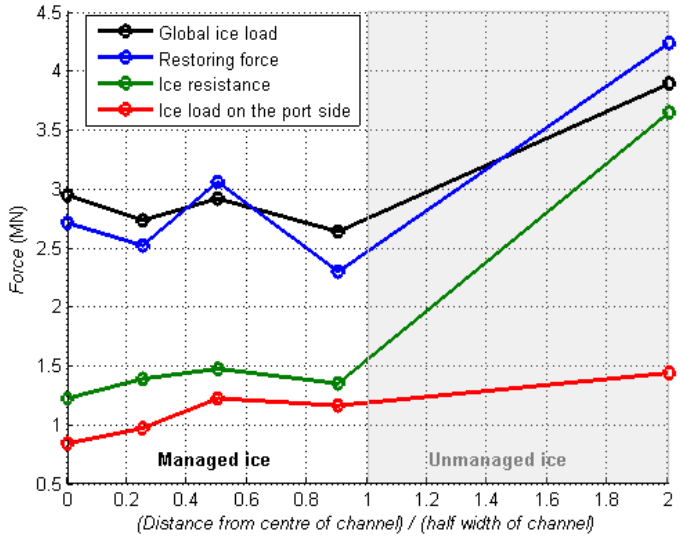

Figure 9. Force components (95th percentile of the global ice loads, restoring force, ice resistance and ice load on the port side of the vessel) as a function of relative horizontal position of vessel with respect to the centre of the managed ice channel

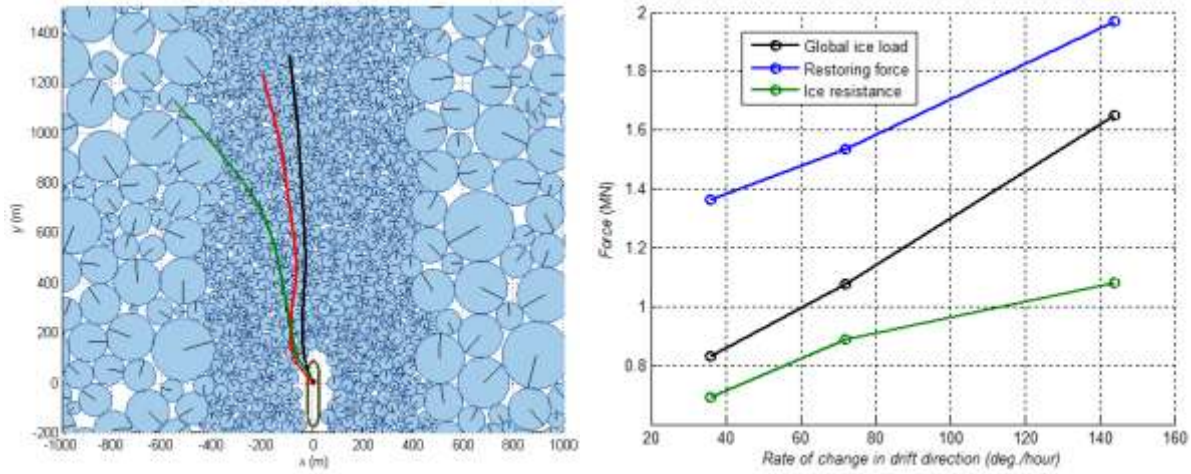

(a) (b)

Figure 10. (a) Resulting 'virtual' trajectories of the vessel based on the applied ice drift direction change (same colour code for drift direction rates of change); and (b) magnitude of force components (95th percentile) as a function of the drift direction rate of change

Complete loop in ice drift

In the Arctic, ice drift reversals are frequent and operating platforms would experience difficulties staying on station and within the managed ice channel as this happen (Rossiter and McKenna, 2013). A test case was performed in which the current was set to make a complete

reversal, as shown in Figure 11. The purpose of this test case is to look at how the ship reacts to fast changes in currents. The same loop was made in open water to highlight the influence the ice had on the movements of the vessel. The excursion for those two cases is shown in Figure 12. The case in ice has greater excursion values, generally.

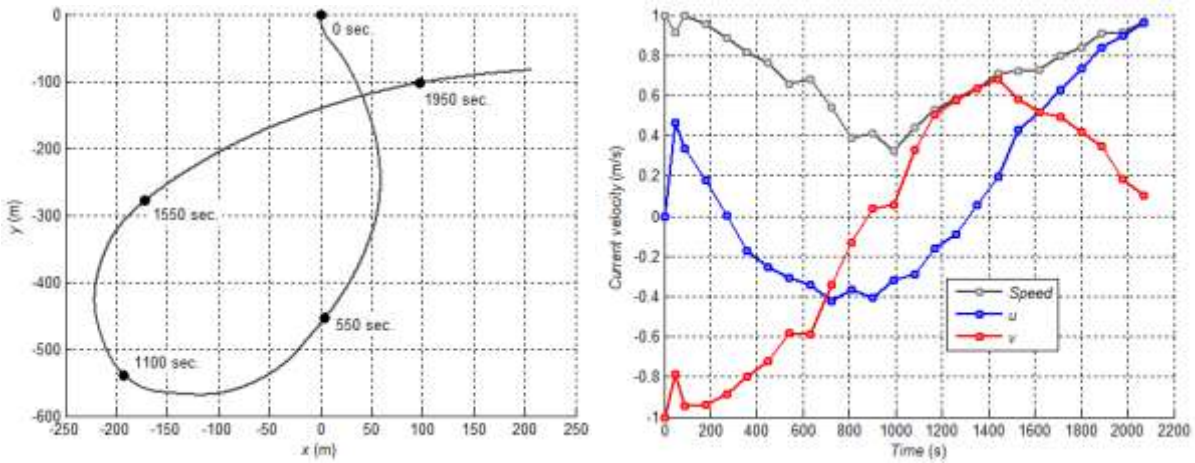

(a) (b)

Figure 11. (a) Trajectory by an ice floe for the scenario where the current completed a loop (times indicated refer to Figure 13); and (b) current velocity components applied corresponding to this loop

Compared with observed ice drift reversals, the loop modelled was relatively short in duration and the magnitude of the current was relatively high, thus producing a small loop. During the time of the simulation, the vessel did not leave the managed ice channel. In real cases (ice reversals are much longer) the vessel can potentially move out of the managed ice channel. Figure 13 shows the configuration of the ice-vessel system at different times in the simulation. When referring to the drift (Figure 11), it is observed that the vessel is slow to respond to drift direction change and that significant differences in the ice loading regime can be expected when this happens (for example, in Figure 13d, the current is offset by more than 90° from the vessel heading and the loading on the vessel is predominantly on the starboard side – loading on the sides of the vessel have the potential to be much higher given sufficient confinement).

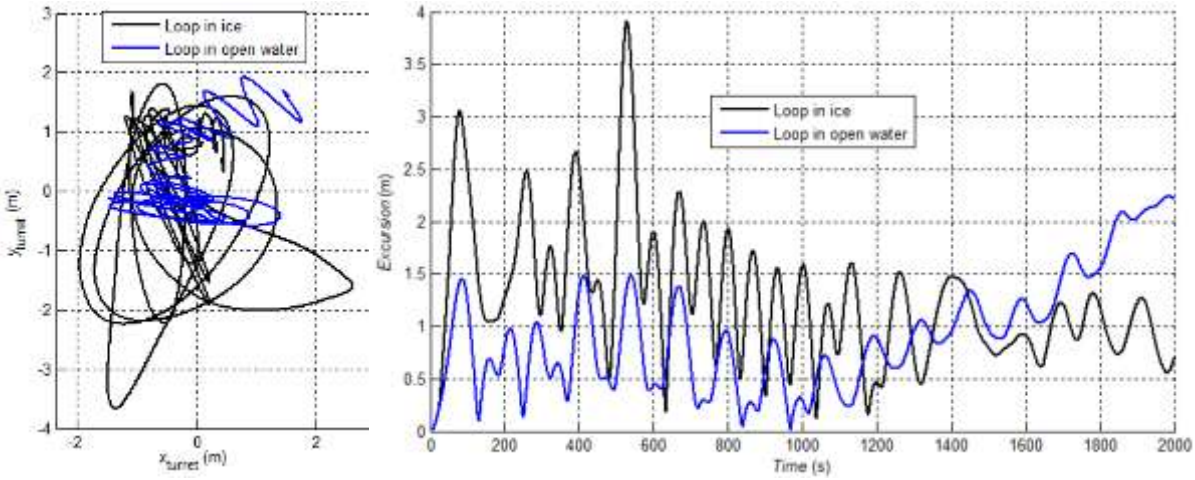

(a) (b)

Figure 12. (a) Turret position throughout the entire simulation; and (b) excursion time trace for the loop ice drift direction with and without ice

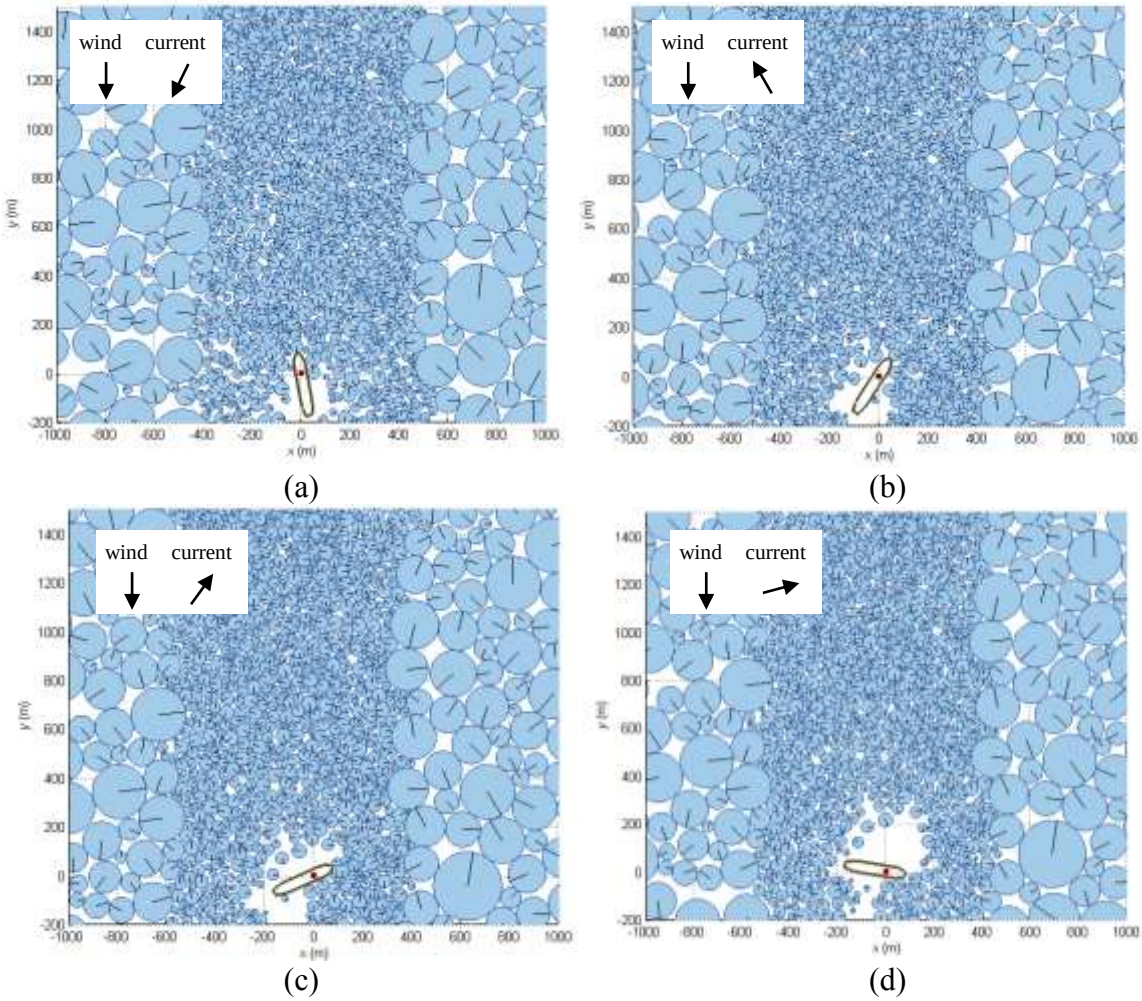

Figure 13. Simulation states at (a) 550 s.; (b) 1100 s.; (c) 1550 s.; and (d) 1950 s. (see Figure 11 for corresponding position at these times)

CONCLUSIONS

The ice loads on a moored vessel in managed ice were simulated using a 2D discrete element model. In this project, the focus was to analyze the influence of important parameters on loads. The effect of (1) floe size and distribution; (2) stiffness of the station-keeping system; and (3) changes in ice drift direction were examined. The main conclusions can be summarized as follows:

- For a given floe diameter distribution, with ice drift parallel to the vessel heading:
  - the magnitude of the excursions generally increase with the largest floes (distribution cutoff) representing the level of ice management;
  - ice resistance and global ice loads increase with larger upper cutoffs;
  - ice loads on the sides of the vessel do not seem sensitive to upper cutoffs.
- When considering unmanaged ice, larger floe diameter distributions increase the ice resistance, the global ice loads and the restoring force. The ice loads applied on the sides of the vessel do not exhibit as much of an increase.
- An increased effective mooring stiffness reduces significantly the excursion. The restoring forces do not seem to be significantly affected by the mooring stiffness.
- Ice resistance and global ice loads were not affected by the mooring stiffness.
- The ratios of the frequency peaks in the excursion power spectrum for different values of mooring stiffness were very close to the expected theoretical value. One

interpretation of this is that the ice does not affect the dynamic behaviour of the mooring system significantly.

- The proximity of the vessel in a managed ice channel to the unmanaged ice does not significantly affect the ice resistance, the global ice loads and the restoring forces. The ice loads on the side of the vessel that is closer to the unmanaged ice increases slightly with the proximity of bigger, unmanaged floes.
- Higher drift direction rates of change may lead to a change in the ice loading regime, such that the vessel may be unable to weathervane with the ice drift and end up in unmanaged ice and the loading on the sides of the vessel may change significantly.

Future work will include using a more realistic model for ice-ice and ice-ship collisions; using a more realistic local shape for the ice floes (the circular assumption may yield unrealistic general behaviour of the ensemble); addressing issues resulting of the two-dimensional assumption (rafting, lifting and submergence, rubbling, friction of the ice on the underside of the vessel etc.); and using more realistic environmental forcing.

ACKNOWLEDGEMENTS

The authors would like to thank Dr. Mark Fuglem, Chris Rossiter, Paul Stuckey and Perry Moore for their help with the model development. This material is based upon work supported by the Ice Management program at the Centre for Arctic Resource Development (CARD), www.card-arctic.com.

REFERENCES

Babić, M., 1988. Discrete particle numerical simulations of granular material behaviour. Report No. 88-11, Department of Civil and Environmental Engineering, Clarkson University, Potsdam, New York, 92 pp.

Cundall, P.A. and Strack, O.D.L., 1979. A discrete numerical model for granular assemblies. Géotechnique, 29 (1): pp. 47–65.

Daly, S.F. and Hopkins, M.A., 1999. Estimating forces on an ice control structure using DEM., Proceedings of the CRIPE 11th Workshop on the Hydraulics of Ice Covered Rivers, Ottawa, ON.

Hansen, E.H. and Løset, S., 1999a. Modelling floating offshore units moored in broken ice: model description. Cold Regions Science and Technology, 29: 97-106.

Hansen, E.H. and Løset, S., 1999b. Modelling floating offshore units moored in broken ice: comparing simulations with ice tank tests. Cold Regions Science and Technology, 29: 107-119.

Hopkins, M.A., 1994. On the ridging of intact lead ice. Journal of Geophysical Research, 99 (C8): 16,351-16,360.

Hopkins, M.A., 2004. A discrete element Lagrangian sea ice model. Engineering Computations, 21 (2/3/4): 409-421.

Keinonen, A.J., Shirley, M., Liljeström, G., and Pilkington, R., 2006. Transit and stationary coring operations in the central polar pack. ICETECH, Paper No. ICETECH06-125-RF.

Journée, J.M.J. and Massie, W.W., 2001. Offshore hydromechanics. First Edition. Delft University of Technology. 570 pp.

Løset, S., 1994a. Discrete element modelling of a broken ice field – Part I: model development, Cold Regions Science and Technology, 22 (4): 339-347.

Løset, S., 1994b. Discrete element modelling of a broken ice field – Part II: simulations of ice loads on a boom. Cold Regions Science and Technology, 22 (4): 349-360.

Munjiza, A., 2004. The combined finite-discrete element method. John Wiley & Sons, ISBN 9780470841990, 348 pp.

Paavilainen, J., Tuhkuri, J. and Polojärvi, A., 2011. 2D numerical simulations of ice rubble formation process against an inclined structure. Cold Regions Science and Technology, 68: 20-34.

Polojärvi, A. and Tuhkuri, J., 2009. 3D discrete numerical modelling of ridge keel punch through tests. Cold Regions Science and Technology, 56(1):18–29.

Rossiter, C. and McKenna, R.F., 2013. Drift direction changes and implications for sea ice management, Proceedings of the 22nd International Conference on Port and Ocean Engineering under Arctic Conditions (POAC), Espoo, Finland (this volume).

Sayed, M., Neralla, V.R. and Savage, S.B., 1995. Yield conditions of an assembly of discrete ice floes. Proceedings of the fifth International Offshore and Polar Engineering Conference, The Hague, The Netherlands, p. 330-335.

U.S. Army Corps of Engineers, 2005. Unified facilities criteria (UFC), Design: Moorings. UFC 4-159-03. 208 pp.

Wright, B., 1999. Evaluation of full scale data for moored vessel stationkeeping in pack ice. PERD/CHC Report 26-200, 120 pp.

Wright, B., 2000. Full scale experience with Kulluk stationkeeping operations in pack ice. PERD/CHC Report 25-44, 141 pp.